Materials Characterization 180 (2021) 111403

Contents lists available at ScienceDirect

Materials Characterization

journal homepage: www.elsevier.com/locate/matchar

Early evolution of δ phase and coarse γ′ phase in Inconel 718 alloy with high temperature ageing

Wei Le [a,b], Zhongwei Chen [a,*], Kang Yan [a], Sufyan Naseem [a], Yanni Zhao [a], Haolan Zhang [a], Zhe Zhang [c]

[a] State Key Laboratory of Solidification Processing, Northwestern Polytechnical University, Xi'an 710072, Shaanxi, China
[b] Langu Institute for Materials Analysis Co. Ltd, Weihai 264207, Shandong, China
[c] School of Materials and Chemical Engineering, Xi'an Technology University, Xi'an 710021, Shaanxi, China

ARTICLE INFO

Keywords:
Inconel 718 alloy
δ phase
Coarse γ′ phase
Hardness

ABSTRACT

The early evolution of the δ phase and coarse γ′ phase in aged Inconel 718 alloy was studied by transmission electron microscope. The results show that the needle-like δ phase first nucleates at the grain boundary and then grows into the grain interior. It is found that two δ phases with different orientations were combined to form one δ phase as the ageing time extended to 4 h. In addition, the δ phase maintains a good orientation relationship with the matrix during ageing. The coarse γ′ phase nucleates at the dislocation, and the increase in size leads to the loss of coherence with the matrix, in which the strengthening effect is not obvious.

1. Introduction

Inconel 718 alloy is a polycrystalline, precipitation-hardened deformed superalloy and has excellent yield strength, creep-, and oxidation-resistance properties at high temperature [1,2]. Due to these excellent properties, Inconel 718 alloy is widely used in aerospace, nuclear energy, petrochemical and other fields with stringent service conditions [3,4]. The properties of alloy are mainly determined via various precipitation phases. Inconel 718 alloy is mainly composed of γ, γ', γ″ and δ phases, in which the face-centered cubic (FCC) phase γ is the matrix phase, nanoscale LI_2-ordered γ' ($Ni_3(Al, Ti)$) and $D0_{22}$-ordered γ″ (Ni_3Nb) are strengthening phases. However, γ″ phase, as a metastable phase, will change to $D0_a$-ordered δ phase (Ni_3Nb) during long term ageing or serviced at high temperatures [5], resulting in a decrease in the strength of the alloy. Due to the effect of this phenomenon, the service temperature of Inconel 718 alloy is lower than 650 °C [6].

As the equilibrium phase of Inconel 718 alloy, the δ phase plays an important role in the mechanical properties of the alloy. On the one hand, the δ phase precipitates at the grain boundary pins the grain boundary and refines grains [7–9], thus improves the strength and ductility of the alloy [10]. Vikram et al. [11]. conducted heat treatment on 718 alloy to precipitate δ phases at the grain boundary and improve the strength of the alloy. On the other hand, δ phase precipitates in grain that can increase the hardness of the alloy by pinning the dislocations and impeding their movement [12]. However, as the volume fraction of the δ phase increases, Nb atoms are rapidly consumed, resulting in a decrease in the volume fraction of the γ′ phase, which adversely affects the properties of the alloy [13–16]. Therefore, it is very important to study the nucleation and growth of the δ phase in detail to control the precipitation of the δ phase.

Researchers have done a lot of research on the precipitation process of the δ phase [13,15,17–19]. Azadian et al. studied the precipitation rate of the δ phase at different temperatures and times, and found that the fastest precipitation rate was around 900 °C [15]. Sundararaman's study showed that at high temperatures, δ phase precipitates directly from the matrix, while at temperatures below 900 °C, δ phase is transformed from pre-existing γ′ phase [13]. According to Ref [13] , δ phase morphology consists of needle-like and blocky (or plate-like). The needle-like δ-phase is precipitated at grain boundaries, while the blocky δ phase is precipitated within grains. In addition to experimental studies, many researchers have used numerical models to calculate δ phase precipitation [20,21]. Low et al. combined the finite element and Kampmann-Wagner numerical model to predict the precipitation state of the δ phase and the predicted results were in good agreement with the experimental results.

In addition to fine γ′ phase precipitation, heterogeneous precipitate of coarse γ′ phase also occurs during the two-stage ageing process [22,23]. The coarse γ′ phase needs to consume a large amount of Nb element, and

* Corresponding author.
E-mail address: chzw@nwpu.edu.cn (Z. Chen).

https://doi.org/10.1016/j.matchar.2021.111403
Received 20 June 2021; Received in revised form 10 August 2021; Accepted 20 August 2021
Available online 23 August 2021

Table 1
Chemical composition of hot-rolled Inconel 718 alloy.

Elements	Ni	Cr	Ti	C	Al	Mo	Si	Nb	Co	Fe
Wt%	52.89	17.25	0.95	0.02	0.49	2.87	0.09	5.07	0.02	Bal.

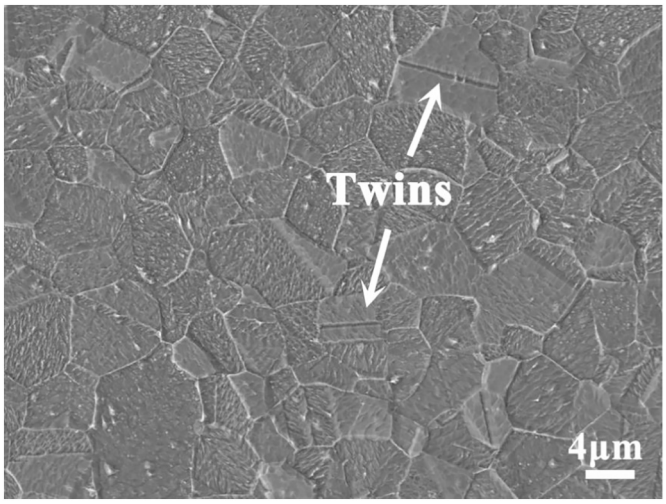

Fig. 1. SEM image of Inconel 718 alloy in as-received condition perpendicular to the rolling direction.

the dislocation provides a channel for the diffusion of Nb element, so the coarse γ′ phase usually nucleates at dislocation [23]. In addition to the conventional ageing process, the coarse γ′ phase can be precipitated during 900 °C heat treatment, and with time, the coarse γ′ phase is completely replaced by the δ phase [13].

In recent years, although the precipitation of these two phases has been reported, their early nucleation and growth processes have not been reported enough. Especially for the coarse γ′ phase, little attention has been paid to the early precipitation process. This paper aims to study in detail the early evolution of the δ phase and coarse γ′ phase during high temperature ageing via transmission electron microscope (TEM). Emphasis is placed on studying the precipitation of morphology, orientation relationship with matrix and its effect on mechanical properties of two phases.

2. Experience procedures

The materials used in the present work were hot-rolled Inconel 718 alloy bars with a diameter of 11 mm and the chemical composition of the alloy given in Table 1. Fig. 1 shows the microstructure of as-received materials perpendicular to the rolling direction. From the image it can be observed that alloy consists of equiaxed grain and a small number of twins. In order to study the early precipitation behavior of δ phase and coarse γ″ phase, specimens were firstly dissolved for 30 min at 1100 °C to form single austenite, then cooled in water. Subsequently, materials were aged for four different times (0.2 h, 0.5 h, 1 h, 4 h) at 900 °C to obtain the sample containing δ phase and coarse γ″ phase precipitated at the early stage.

Samples for Scanning electron microscope (SEM) were ground in metallographic sandpaper from 400 to 2000, and then mechanically polished to no visible scratches. After that, samples were chemical-etched in solution (5 g CuCl+100 ml HCl + 100 ml C_2H_5OH) at room temperature. All the metallographic investigations and microstructure analyses were performed in Zeiss Sigma 500 equipped with field emission gun electron source (FEG). Working distance was chosen 8.5 mm and accelerating voltage was 15 KV with a 30 μm standard aperature.

TEM specimens were cut from the aged alloy bar by electrodischarge machining and mechanically ground to about 50 μm thick. TEM-foils were then thinned by Gatan 657 Dimple Grinder and Gatan 695 PIPS II: Precision ion polishing system produced by Gatan Corporation of the United States. All transmission electron microscopy (TEM) bright field (BF) images, selected area electron diffraction (SAED) images and high-resolution transmission electron microscopy (HRTEM) images were recorded with a ThermoFisher Talos F200S at 200 kV acceleration voltage. High-angle annular dark-field (HAADF) and energy-dispersive X-ray spectroscopy (EDXS) were acquired using ThermoFisher Themis Z aberration-corrected TEM at 300 kV acceleration voltage with four energy spectrum probes.

Microhardness of each sample was conducted via EDHV-1000

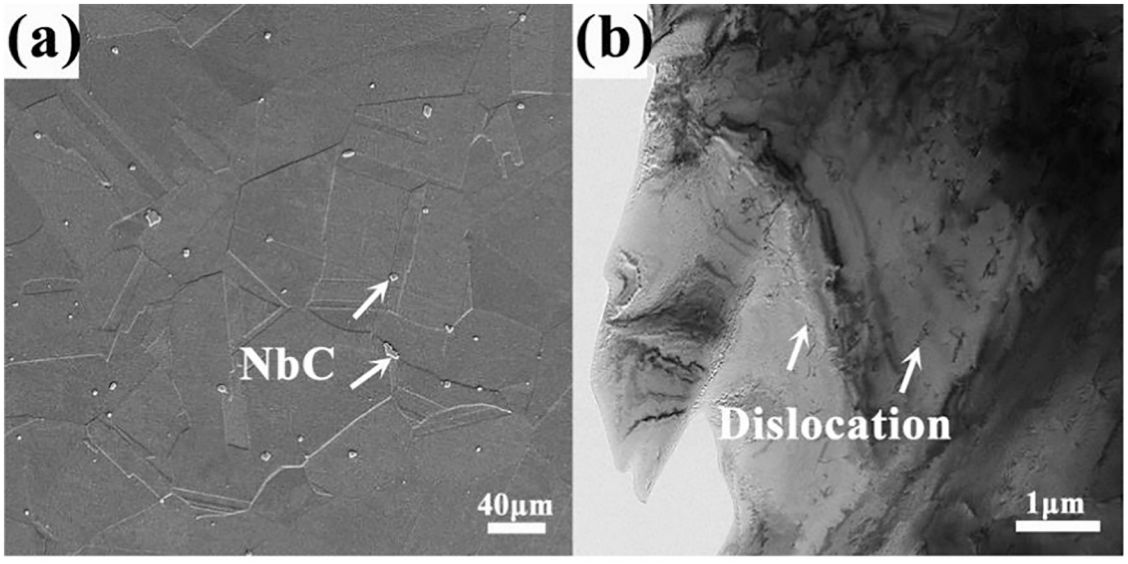

Fig. 2. Microstructure of Inconel 718 alloy after solution treatment.

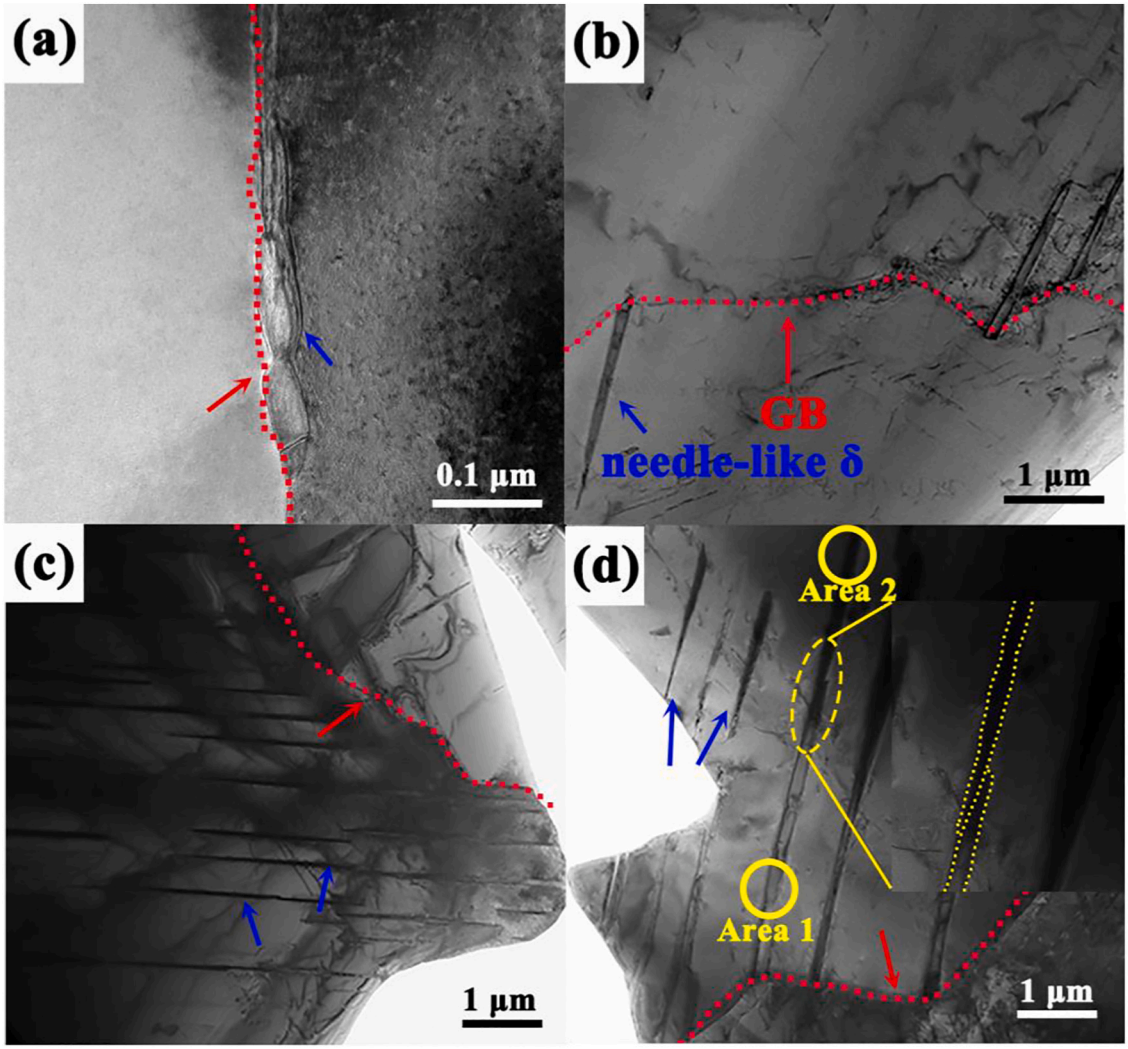

Fig. 3. TEM BF image near grain boundary: (a) 900 °C/0.2 h; (b) 900 °C/0.5 h; (c) 900 °C/1 h; (d) 900 °C/4 h.

according to ASTM E92–82 [23]. The force used was 300 g and the loading time was 15 s. In order to reduce the experimental error, each sample, which was mechanically ground and polished on the surface where there was no obvious scratch, was measured five times to obtain the average hardness.

3. Results and discussion

For the convenience of analysis, the microstructure of Inconel 718 alloy after solution treatment was observed. Fig. 2a shows a SEM image of the alloy after solution treatment. Compared with as-received condition, the grains grow significantly after solution treatment, and a small amount of NbC particles and thermal twins appear in the alloy. In Fig. 2b, there are no other precipitates in the matrix, but a few dislocations occur, as a highlight by the white arrow in the figure. It has been suggested that dislocations are introduced to the γ-matrix via stresses generated during quenching [24], and these dislocations may provide nucleation sites for δ phase or coarse γ″ phase [23,25].

3.1. Nucleation and growth process of δ phase precipitation

In order to investigate the early evolution of δ phase morphology, TEM BF images of Inconel 718 alloy near grain boundary after different time ageing were firstly acquired, as shown in Fig. 3. Grain boundary and needle-like δ phase are highlighted by red and blue arrows, respectively. It can be seen in Fig. 3a that a small amount of δ phase is nucleate at the grain boundary after 900 °C/0.2 h ageing. The result coincides with the works Sundararaman [18] and Azadian [14] that needle-shaped, elongated particles of the δ phase were found to have nucleated at the austenite grain boundaries. Because grain boundary provides good thermodynamic and kinetic conditions, needle-like δ phase nucleation occurs at the grain boundary. In Fig. 3b, a small number of needle-like δ phases have appeared and are growing from the grain boundary into the grain. In addition, it is clear that the growth direction of needle-like δ phases formed big angle with grain boundary, which has also been found by Sundararaman et al. [13] According to Ref. [13], during the growth process, needle-like δ phases tend to be larger angle with grain boundary because they cannot find a suitable habitus surface that is parallel to the grain boundary. In Fig. 3c corresponding to a 900 °C/1 h, in addition to some δ phases that grow from grain boundaries into the grain, many δ phases also appear far from the grain boundaries and grow in the same direction as the δ phases nucleating at grain boundaries. After 900 °C/4 h aged (Fig. 3d), the needle-like δ phase grows further and the width and length of the needle-like δ phase increase as well.

From Fig. 3d, it revealed that one δ phase has two variations with different habit plane. For convenience, a variant close to the grain boundary is called variant A, and far away is called variant B. The yellow

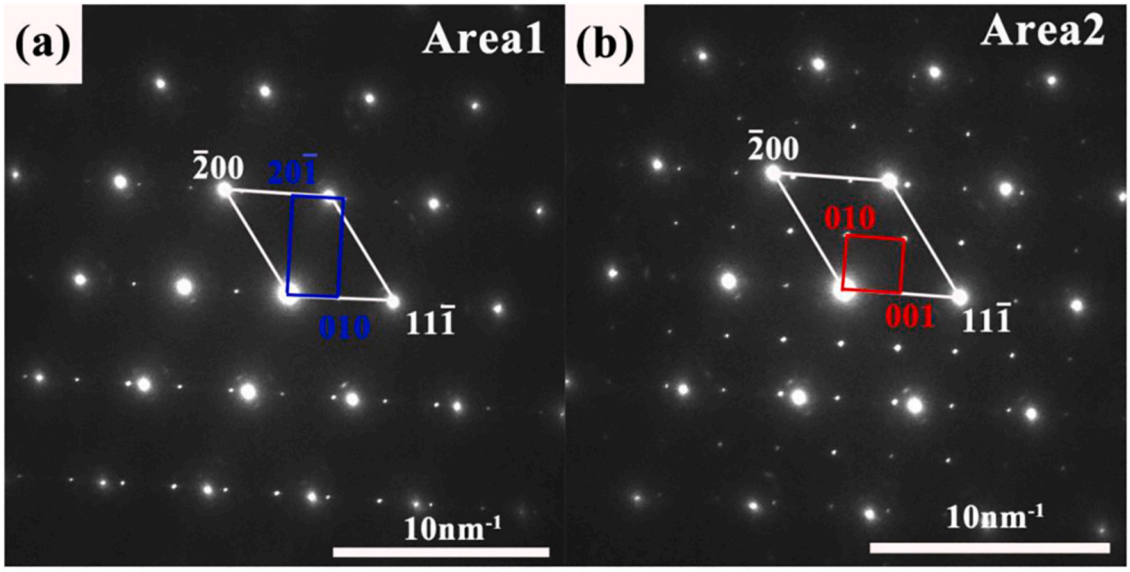

Fig. 4. The SAD patterns image: (a) corresponding area 1; (b) corresponding area 2.

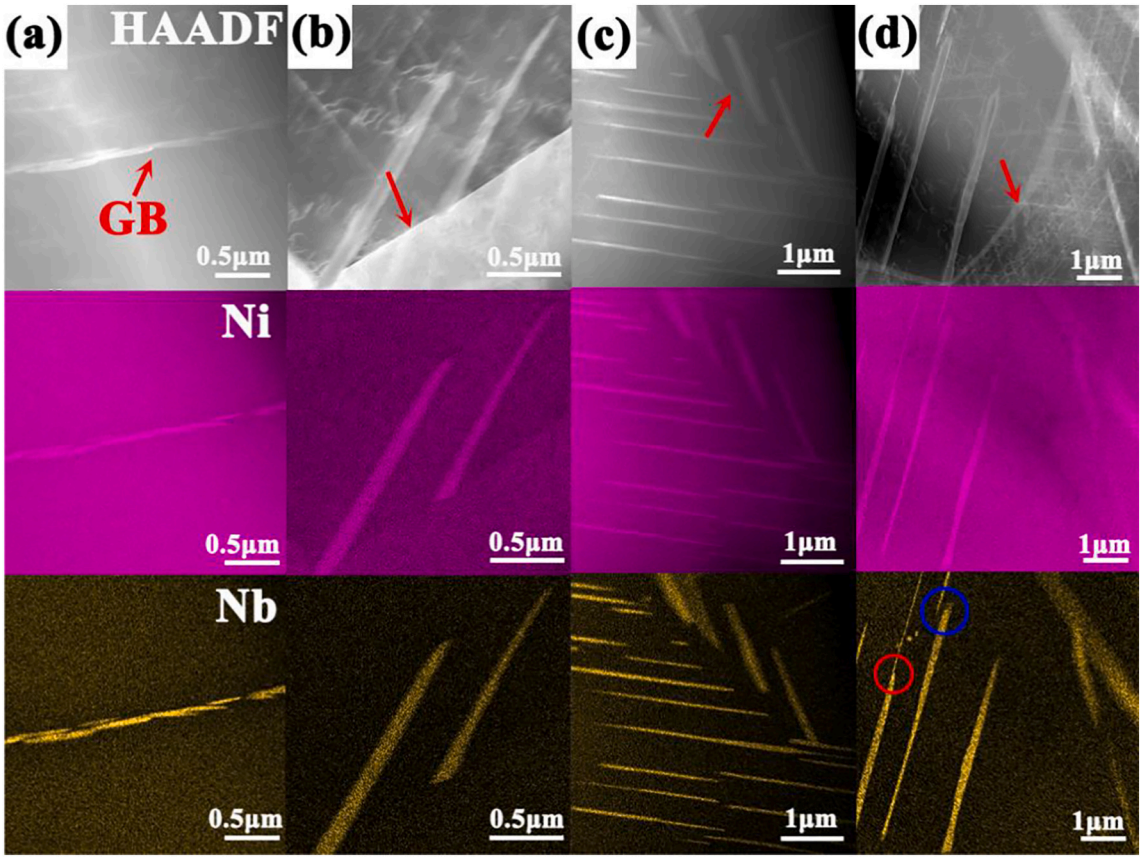

Fig. 5. HAADF and EDXS maps of different ageing time near the grain boundary: (a) 900 °C/0.2 h; (b) 900 °C/0.5 h; (c) 900 °C/1 h; (d) 900 °C/4 h.

dotted line in the figure indicates where the two variants are connected and the accompanying image in Fig. 3d is a larger version of the area circled by the yellow dotted line. In addition, SEAD analysis on the two variants shows that two variants have different selected area diffractions (SAD) patterns, as shown in Fig. 4. These phenomena suggest that two variants δ phases combine to form a single δ phase when one δ variant encounters another δ variant with different habit plane during growth. This result was also obtained by Sundararaman et al. through detailed SEM examination of deeply etched δ specimens, and this growth mechanism is called the Envelope Mechanism [17].

Fig. 4 shows SAD patterns of two different areas observed along the $[011]_\gamma$ direction, in which area 1 and area 2 contain parts of variant A and variant B, respectively. In Fig. 4a, corresponding to variant A, it can be seen that SAD patterns were composed of two sets of spots, in which the main spots are the matrix spots and the additional spots correspond δ phase. Furthermore, the addition spots were easily identified as the ones

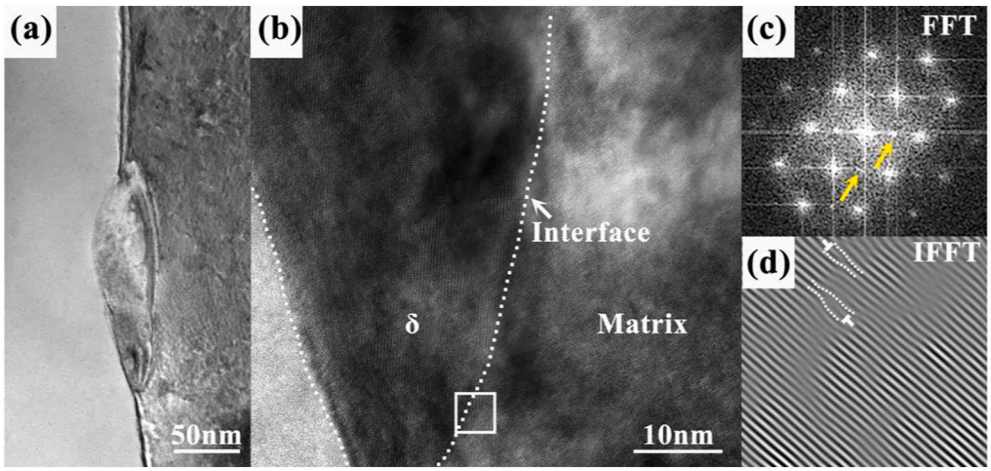

Fig. 6. TEM investigation for 900 °C/0.2 h aged sample: (a) BF image showing intercrystalline δ phase; (b) HRTEM image for δ phase and matrix; (c), (d) Corresponding FFT and IFFT images of area cycled by the white box in (b), respectively.

corresponding with the $[102]_{\delta}$ zone axis. Therefore, the crystallographic orientation relationship between variant A and matrix can be expressed as $[102]_{\delta A}//[011]_{\gamma}$ and $(010)_{\delta A}//(11^{-}1)_{\gamma}$. Fig. 4b shows the SAD patterns in area 2 under the same conditions. Like Fig. 4a, Fig. 4b also contains two sets of patterns. However, what is different from Fig. 4a is that the additional spots in Fig. 4b are indexed as the ones corresponding with the $[100]_{\delta}$ zone axis. Thus, the crystallographic orientation relationship between variant B and matrix can also be expressed as $[100]_{\delta B}//[011]_{\gamma}$ and $(001)_{\delta B}//(11^{-}1)_{\gamma}$.

Fig. 5 shows EDXS mapping at grain boundary with different time ageing. The maps for Ni and Nb are shown in pink and claybank, respectively. After 900 °C/0.2 h ageing (Fig. 5a), it is obvious that the two elements have segregation at the grain boundary, and these elements are the forming elements of the δ phase, indicating that the nucleation of needle-like δ phase occurs at the grain boundary. However, with the depletion of Nb near the grain boundary, Nb elements are insufficient to provide conditions for the δ phase to continue growing along the grain boundary. Therefore, with the extension of ageing time, needle-like δ phases keep growing into the grain, as shown in Fig. 5b. In Fig. 5c, a needle-like δ phase appears on both sides of the grain boundary and grows inwards at a certain angle. After 900 °C/4 h ageing corresponding to Fig. 5d, the number of needle-like δ phases is less than that in Fig. 5c. In addition, there is a significant difference in the thickness of the two stages of one δ phase and the proximity of the two δ phases, circled by the red and blue respectively, which indicates that two δ phases combine to form one after 4 h ageing.

3.2. Interface between γ matrix and δ phase

Generally speaking, the δ phase is precipitated incoherently at grain boundaries (or twin boundary) [13,17]. However, in the course of our research, we found some differences from those reported in these references. Therefore, the interface between the δ phase and matrix after different aged time was investigated.

In order to observe the interface change between the δ phase and matrix with the growth of the δ phase, a detailed TEM investigation was firstly applied on a 900 °C/0.2 h aged sample. Fig. 6a presents the BF image of the aged sample. δ phase (~178 nm in length and ~ 40.9 nm in width) heterogeneously nucleated and grown at grain boundaries. Fig. 6b shows the HRTEM image near the grain boundary, where the middle part of two white dotted lines is δ phase, the matrix on the right and another grain on the left. The results (cf. Fig. 6c) of Fast Fourier transformation(*FFT*)at the interface (cycled by white box area in b) show that the orientation relationship between δ phase and the matrix is $[011]_{\gamma}//[102]_{\delta}$ and $(010)_{\delta}//(11^{-}1)_{\gamma}$, which is exactly corresponding to the results in Fig. 4a. Inverse Fast Fourier Transforms (IFFT) was further performed on the white box region in b, as shown in Fig. 6d, and it can be seen that redundant semi-atomic surfaces appeared on both sides of

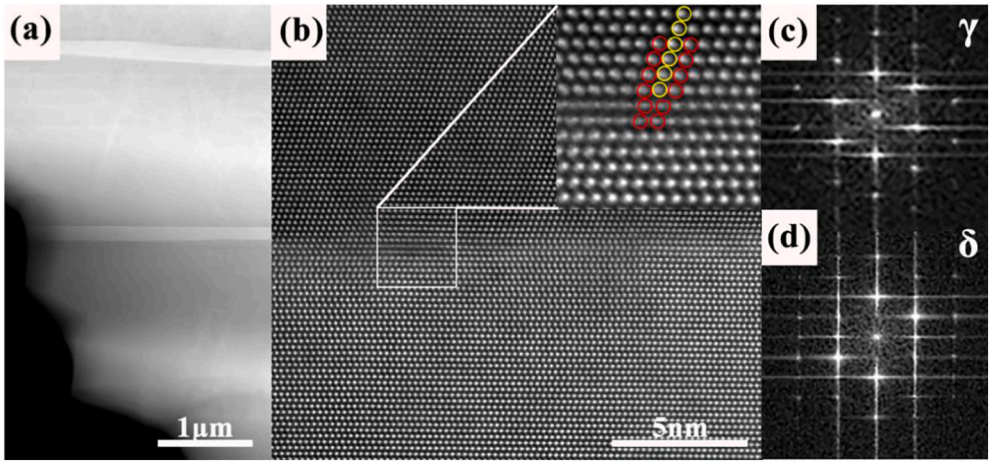

Fig. 7. STEM investigation for 900 °C/4 h ageing sample: (a) HAADF image showing needle-like δ phase; (b) HRSTEM image for δ phase and matrix; (c) and (d) Corresponding FFT of δ phase and γ matrix, respectively;

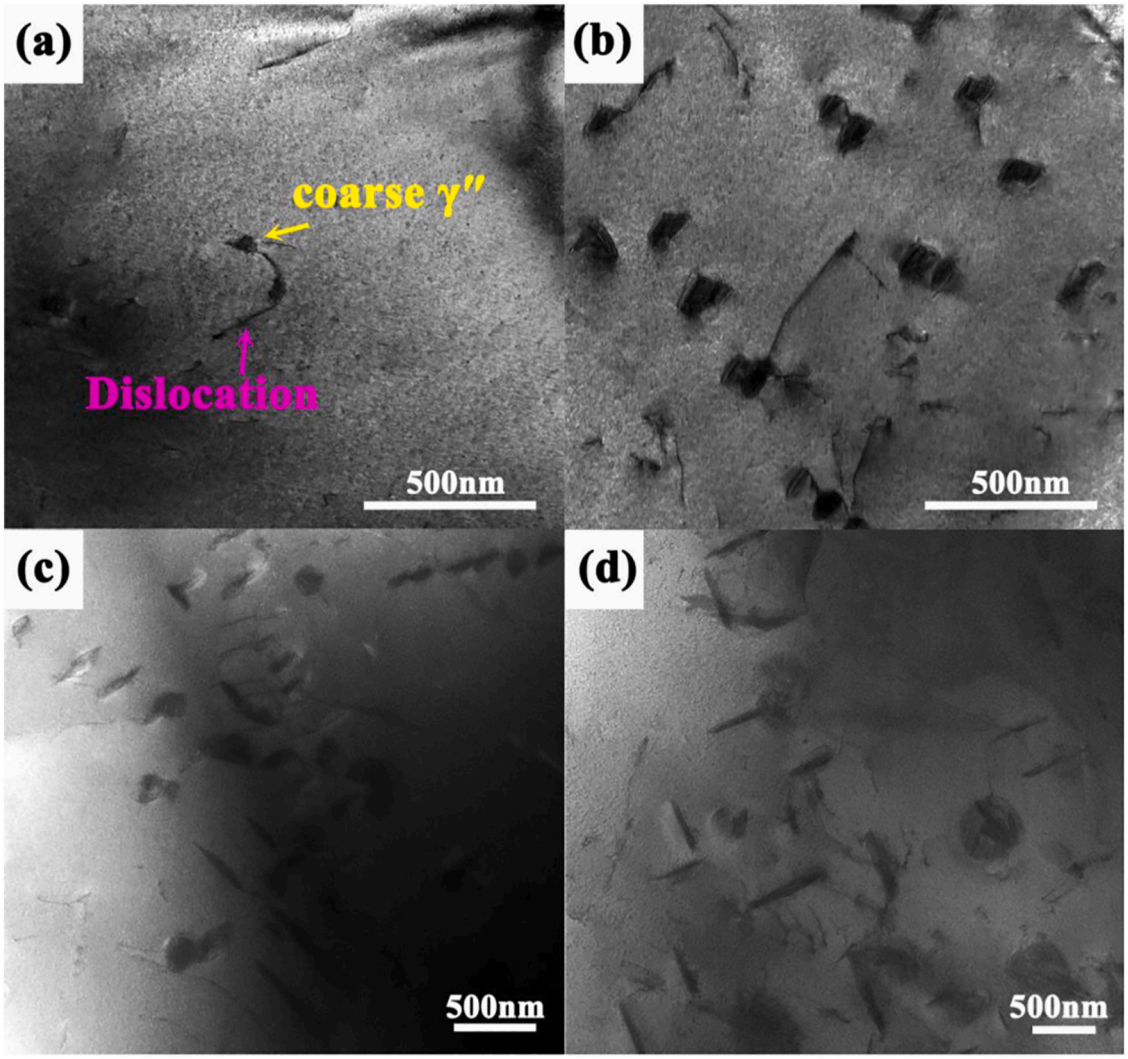

Fig. 8. TEM BF image inside grain, (a) 900 °C/0.2 h; (b) 900 °C/0.5 h; (c) 900 °C/1 h; (d) 900 °C/4 h.

the δ phase and the matrix. Examination of the HRTEM and the IFFT image indicated that the interface between the δ phase and matrix was semi-coherent after 900 °C/0.2 h aged.

In order to observe the interface between the δ phase and matrix after a long time of ageing, HAADF and HRSTEM were used to analyze the samples after 900 °C/4 h aged, and the results were presented in Fig. 7. HAADF image in Fig. 7a shows the elongated δ phases parallel to each other are heterogeneously distributed in the matrix. The correlating HRSTEM image in Fig. 7b exhibits atoms arrangement of matrix, δ phase and their interface. It can be seen that the matrix and δ phase show a coherent relationship in most areas, while atomic misarrangement occurs only in a few places, as shown in the accompanying figure in b. Therefore, after aged at 900 °C/4 h, the δ phase still shows a semi-coherent relationship with the γ matrix. Fig. 7a and b are FFT images of matrix and δ phase in b, which are [011] axis of matrix and [102] axis of δ phase, respectively.

By comparing the interface between the δ phase and matrix after ageing at 900 °C for 0.2 h and 4 h, it is found that both of them are semi-coherent. In other words, the interface between δ phase and the matrix does not change after aged for a period of time.

3.3. Nucleation and growth process of coarse γ′ precipitation

The BF images from TEM for coarse γ′ phase after different aged time are shown in Fig. 8. In the insert of Fig. 8a, corresponding to a 900 °C/0.2 h, a small number of dislocations and primary coarse granular γ′ phase appear within the grain, indicated by pink and yellow arrows, respectively. Additionally, it is notable that the coarse γ′ phase heterogeneously precipitates on the dislocation line. After 900 °C/0.5 h ageing, as shown in Fig. 8b, it can be seen that a large number of primary γ′ phase precipitates. Meanwhile, the average size of coarse γ′ is 85.4 nm by measurement and calculation, which is larger than coarse γ′ with 0.2 h aged (~53.9 nm). With prolonging ageing time, the primary coarse γ′ phase continuously grows, and the morphology changed from granular to disc, as can be seen in Fig. 8c and d.

Unlike the fine γ′ phase, the coarse γ′ phase usually nucleates at the dislocation [23]. On the one hand, due to the slow diffusion of Nb elements in the matrix [26], dislocations can provide a diffusion channel for Nb elements, thus improving the diffusion rate of Nb element. On the other hand, misfit strain or chemical coupling between Ni atoms and matrix can be reduced by the diffusion of the stress field near the dislocation to the matrix lattice [27]. As can be seen from Fig. 8, the coarse γ′ phase nucleates at the dislocation, and grows continuously with the extension of ageing time.

According to the transformation–time–temperature (TTT) curve, there is an overlap region between the δ phase and γ′ phase near 900 °C [28]. In this temperature range, γ′ phase precipitates preferentially to δ phase, and with the extension of ageing time, γ′ phase gradually

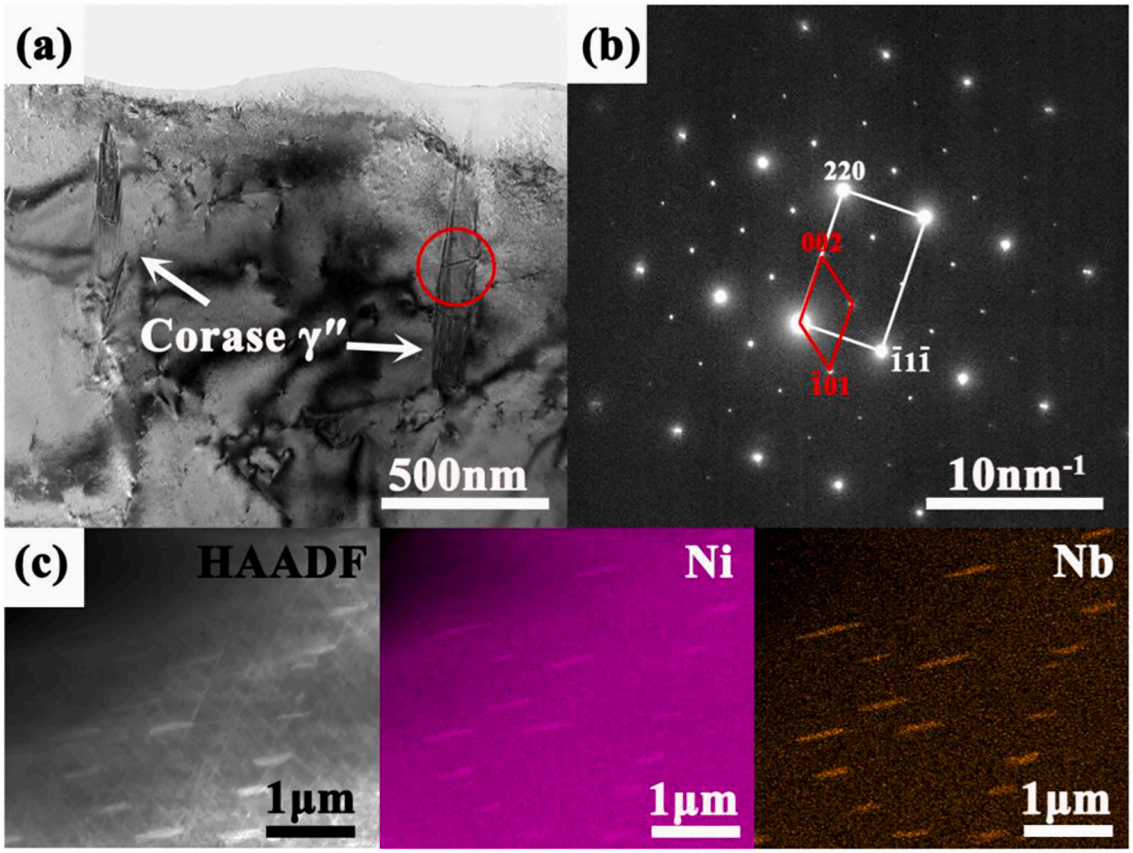

Fig. 9. SAD patterns and EDXS results of coarse γ′ phase after 900 °C/4 h aged, (a) BF image showing coarse γ′, (b) diffraction pattern of coarse γ′ phase, and the pattern was taken in [$\bar{1}$12] zone axis direction, (c) EDXS maps investigation for coarse γ′ precipitates.

transforms to δ phase. Sundraraman et al. [13] studied the evolution of microstructure during ageing at 900 °C for different times and found that after 20 h of aged, a large number of coarse γ′ phase would appear, but after 100 h of aged, γ′ phase disappeared and only δ phase existed. In this work, the maximum ageing time is 4 h, so only the γ′ phase appears inside the grain, but no δ phase is found.

Fig. 9 presents SAD patterns and EDXS results of coarse γ′ phase after 900 °C/4 h aged. In Fig. 9a, coarse γ′ phases heterogeneously distributed in the matrix, indicated by the white arrow. Electron diffraction analysis was performed on the red circle region in Fig. 9a along with the [$\bar{1}$12] zone axis direction, and the result is shown in Fig. 9b. It can be seen that SAD patterns were composed of two sets of spots, in which the main spots are the matrix spots and the additional spots correspond to γ′ phases. Therefore, the crystallographic orientation relationship between coarse γ′ phase and matrix can be expressed as $[\bar{1}12]_{\gamma}//[010]_{\gamma'}$ and $(220)_{\gamma}//(002)_{\gamma'}$. Fig. 9c shows EDXS maps of HAADF, Ni and Nb elements, clearly showing that Nb element has a strong tendency to be divided into coarse γ′ phases.

3.4. Interface between γ matrix and coarse γ′ phase

Fig. 10 presents the STEM and EDXS analysis for the coarse γ′ phase in the sample after 900 °C/4 h aged. HAADF image in Fig. 10(a) shows a coarse γ′ phase obviously precipitated in the matrix. A region was selected from the interface between the coarse γ′ phase and γ matrix for HRSTEM observation, as shown in Fig. 10(b). The accompanying two images are FFT of the left and right parts in the image, which are diffraction spots corresponding to the γ′ phase along [010] zone axis and γ matrix along [$\bar{1}$12] zone axis, respectively. In addition, no atomic disarrangement was found between γ′phase and γ matrix phase. Atomic EDXS maps of the coarse γ′ phase are provided in Fig. 10(c). The maps for Nb and Ni are shown in green and blue, respectively. It is clear that there is an Nb atom for every three Ni atoms along with the (001) direction of the γ′ phase.

Many studies have shown that the fine γ′ particles are completely coherent with the γ matrix in the Inconel 718 alloy [23,29–31]. However, with the increase in size, γ′ particles will deviate from the rule [32]. The increase in size will lead to the continuous increase of stress at the interface between the γ′ phase and γ matrix. When the size reaches a critical value, line dislocations will be generated at the interface to release the stored stress, which will lead to the loss of coherence. According to the Ref. [24], the critical size of the lost coherence of the γ′ phase was predicted to be 91 nm and 140 nm via the stability and energy criterion, respectively. In this work, the size of the coarse γ′ phase after ageing at 900 °C/4 h obviously exceeds the two predicted sizes. However, it can be seen from Fig. 10b that there is no atomic disarrangement on either side of the interface. Due to the limitations of the experiment, it is impossible to characterize the entire γ phase and matrix interface. Therefore, the interface between the γ phase and matrix can only be defined as coherent but not fully coherent in this work.

3.5. Hardness testing

Fig. 11 shows the curve of the hardness value of Inconel 718 alloy changing with the ageing time. The average hardness of alloy after solution treatment is 189.44 HV. It can be seen from the figure that the hardness of the alloy increases with the extension of ageing time. However, the increase of hardness value is not very significant, and the hardness of the material after 4 h aged is only 37.06 HV higher than that after solid solution, indicating that the improvement of the hardness of the coarse γ′ alloy is not obvious.

For most alloys, precipitation strengthening is the main

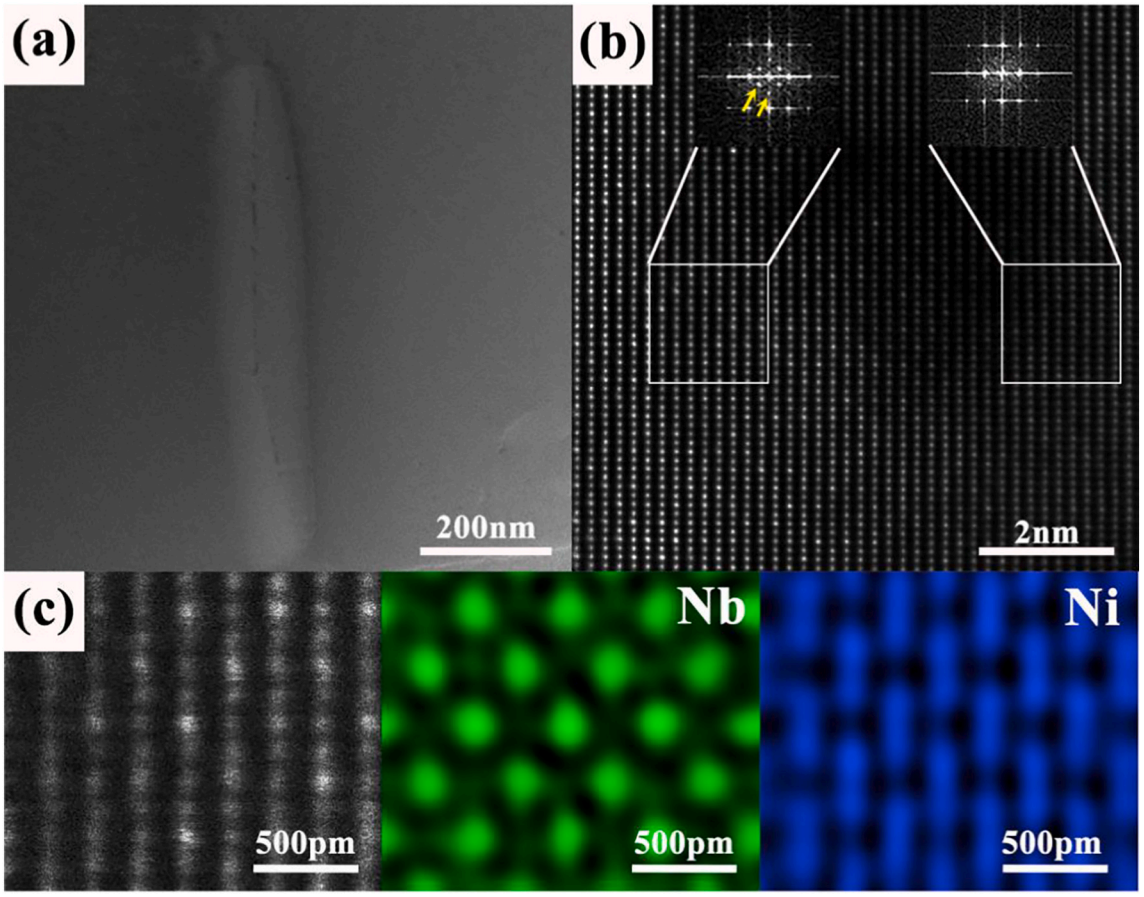

Fig. 10. STEM-EDXS investigation for coarse γ′ precipitate, (a)HAADF image showing coarse γ′ phase, (b) HRSTEM image for coarse γ′ phase and matrix, (c)EDXS mapping images for coarse γ′ phase.

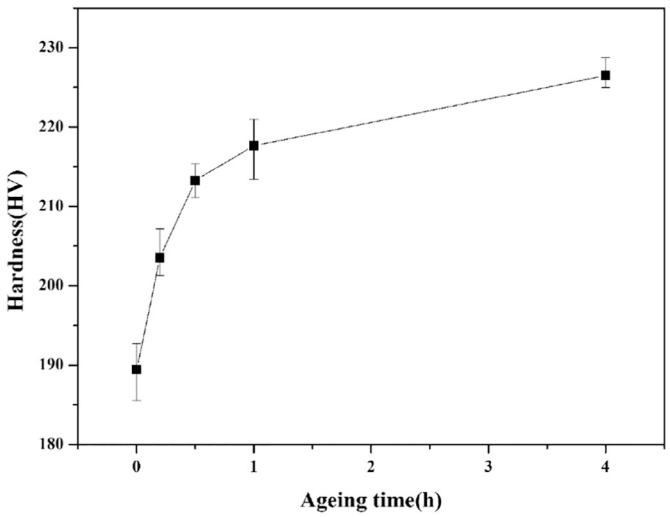

Fig. 11. Hardness evolution of Inconel 718 alloy as aged time.

strengthening method [33–36]. The strengthening mechanism of the precipitated phase is to increase the strength of the alloy by hindering the dislocation motion. However, this hardening effect depends largely on the condensed state of the precipitated phase in the matrix [37]. The strengthening effect of the precipitated phase is the best when the precipitated phase is coherent with the matrix and the mismatch strain between the two phases is within the elastic range. On the contrary, when the precipitates and the matrix are semi-coherent or incoherent, the strengthening effect will decline [32]. Therefore, with the prolonging of ageing time, the content of the γ phase and the hardness of the alloy increases. However, due to the loss of coherence between the γ′ phase and matrix, the strengthening effect is not obvious.

4. Conclusions

In this work, the early evolution of the δ phase and coarse γ′ phase after ageing at 900 °C has been studied in detail by transmission electron microscopy. The nucleation and growth of the δ phase and coarse γ′ phase, as well as the orientation and interface with matrix have been systematically investigated. Based on the experimental results, the following conclusions are drawn:

(1) The δ phase first nucleated non-uniformly at grain boundaries and then grown from the grain boundary into the grain. After ageing at 900 °C/4 h, it was found that two δ phases with different orientations were combined to form one δ phase.
(2) During the short-time ageing process, the interface between the δ phase and matrix remains semi-coherent. The δ phase has two orientations relationship with the matrix, respectively:

OR1: $[102]_\delta//[011]_\gamma$ and $(010)_\delta//(11^{-}1)_\gamma$.
OR2: $[100]_\delta//[011]_\gamma$ and $(001)_\delta//(11^{-}1)_\gamma$.

(3) Coarse γ′ phase nucleated at the dislocation, and the morphology changed from grain to short rod shape with the prolongation of aged time. After aged at 900 °C for 4 h, the coarse γ′ phase has a coherent relationship with the matrix. Moreover, their

orientations relationship corresponds to $[\bar{1}12]_{\gamma}//[010]_{\gamma'}$ and $(220)_{\gamma}//(002)_{\gamma'}$.

(4) The loss of coherence between coarse γ′ phase and matrix results in the insignificant increase in hardness of the alloy. After 900 °C/4 h ageing, the hardness of alloy is only 37.06 HV higher than that of the solid solution state.

Declaration of Competing Interest

The authors declare that they have no known competing financial interests or personal relationships that could have appeared to influence the work reported in this paper.

Acknowledgement

The authors gratefully acknowledge financial support from the National Key R&D Program of China (NO.2018YFB1900100) and the National Natural Science Foundation of China (NO.51674204).

References

[1] W. Chen, M.C. Chaturvedi, The effect of grain boundary precipitates on the creep behavior of Inconel 718, Mater. Sci. Eng. A 183 (1994) 81–89.
[2] R.B. Li, M. Yao, W.C. Liu, X.C. He, Isolation and determination for δ, γ' and γ″ phases in Inconel 718 alloy, Scr. Mater. 46 (2002) 635–638.
[3] R.E. Schafrik, D.D. Ward, J.R. Groh, Application of Alloy 718 in GE Aircraft Engines: Past, Present and Next Five Years, Superalloys, 2001.
[4] J.J. Debarbadillo, S.K. Mannan, Alloy 718 for oilfield applications, JOM 64 (2012) 265–270.
[5] M. Dehmas, J. Lacaze, A. Niang, B. Viguier, TEM study of high-temperature precipitation of delta phase in inconel 718 alloy, Adv. Mater. Sci. Eng. 2011 (2011) 1–9.
[6] T. Sugui, S. Haofang, J. Ying, Investigation on γ' to γ″ transition in an IN718G superalloy during heat treatment, using first principle, Mater. Charact. 162 (2020) 110–168.
[7] M. Cheng, H.Y. Zhang, S.H. Zhang, Microstructure evolution of delta-processed IN718 during holding period after hot deformation, J. Mater. Sci. 47 (2011) 251–256.
[8] H.B. Dong, G.C. Wang, Effect of deformation process on superplasticity of inconel 718 alloy, Rare Metal Mater. Eng. 44 (2015) 298–302.
[9] Y.C. Lin, D.G. He, M.S. Chen, X.M. Chen, C.Y. Zhao, X. Ma, Z.L. Long, EBSD analysis of evolution of dynamic recrystallization grains and δ phase in a nickel-based superalloy during hot compressive deformation, Mater. Des. 97 (2016) 13–24.
[10] L.C.M. Valle, L.S. Araújo, S.B. Gabriel, J. Dille, L.H.D. Almeida, The effect of δ phase on the mechanical properties of an inconel 718 superalloy, J. Mater. Eng. Perform. 22 (2012) 1512–1518.
[11] R.J. Vikram, A. Singh, S. Suwas, Effect of heat treatment on the modification of microstructure of selective laser melted (SLM) IN718 and its consequences on mechanical behavior, J. Mater. Res. 35 (15) (2020) 1949–1962.
[12] M. Anderson, A.L. Thielin, F. Bridier, P. Bocher, J. Savoie, δ phase precipitation in inconel 718 and associated mechanical properties, Mater. Sci. Eng. A 679 (2017) 48–55.
[13] M. Sundararaman, P. Mukhopadhyay, S. Banerjee, Precipitation of the δ Ni_3Nb phase in two nickel base superalloys, Metall. Trans. A. 19 (1988) 453–456.
[14] S. Gribbin, S. Ghorbanpour, N.C. Ferreri, J. Bicknell, I. Tsukrov, M. Knezevic, Role of grain structure, grain boundaries, crystallographic texture, precipitates, and porosity on fatigue behavior of Inconel 718 at room and elevated temperatures, Mater. Charact. 149 (2019) 184–197.
[15] S. Azadian, L.Y. Wei, R. Warren, Delta phase precipitation in Inconel 718, Mater. Charact. 53 (2004) 7–16.
[16] S.H. Zhang, H.Y. Zhang, M. Cheng, Tensile deformation and fracture characteristics of delta-processed Inconel 718 alloy at elevated temperature, Mater. Sci. Eng. A 528 (2011) 6253–6258.
[17] M. Sundararaman, N. Sachin, B.S. Jung, V. Amit, P. Bhaskar, R. Kishore, Evolution of δ Phase Microstructure in Alloy 718, TMS, 2010, pp. 737–750.
[18] I. Kirman, D.H. Warrington, The precipitation of Ni_3Nb phases in a Ni-Fe-Cr-Nb alloy, Metall. Trans. A. 1 (1970) 2667–2675.
[19] Y. Huang, T.G. Langdon, The evolution of delta-phase in a superplastic Inconel 718 alloy, J. Mater. Sci. 42 (2007) 421–427.
[20] Z.K. Low, T. Chaise, D. Bardel, S. Cazottes, P. Chaudet, M. Perez, D. Nelias, A novel approach to investigate delta phase precipitation in cold-rolled 718 alloys, Acta Mater. 156 (2018) 31–42.
[21] J.J. Ruan, N. Ueshima, K. Oikawa, Growth behavior of the δ-Ni_3Nb phase in superalloy 718 and modified KJMA modeling for the transformation-time-temperature diagram, J. Alloys Compd. 814 (2020) 152289.
[22] G.H. Cao, T.Y. Sun, C.H. Wang, X. Li, M. Liu, Z.X. Zhang, P.F. Hu, A.M. Russell, R. Schneider, D. Gerthsen, Z.J. Zhou, C.P. Li, G.F. Chen, Investigations of γ', γ″ and δ precipitates in heat-treated Inconel 718 alloy fabricated by selective laser melting, Mater. Charact. 136 (2018) 398–406.
[23] F. Theska, K. Nomoto, F. Godor, B. Oberwinkler, A. Stanojevic, S.P. Ringer, S. Primig, On the early stages of precipitation during direct ageing of Alloy 718, Acta Mater. 188 (2020) 492–503.
[24] M. Sundararaman, P. Mukhopadhyay, S. Banerjee, Some aspects of the precipitation of metastable intermetallic phases in Inconel 718, Metall. Trans. A. 23 (1992) 2015–2028.
[25] W.R. Sun, S.R. Guo, J.H. Lee, N.K. Park, Y.S. Yoo, S.J. Choe, Z.Q. Hu, Effects of phosphorus on the δ-Ni_3Nb phase precipitation and the stress rupture properties in alloy 718, Mater. Sci. Eng. A 247 (1998) 173–179.
[26] M.S.A. Karunaratne, R.C. Reed, Interdiffusion of niobium and molybdenum in nickel between 900–1300 °C, Defect Diff. Forum 237-240 (2005) 420–425.
[27] A. Janotti, M. Krcmar, C.L. Fu, R.C. Reed, Solute diffusion in metals: larger atoms can move faster, Phys. Rev. Lett. 92 (2004), 085901.
[28] C.T. Sims, N.S. Stoloff, W.C. Hagel, Superalloys II: High-Temperature Materials for Aerospace and Industrial Power, 1987.
[29] Y.F. Han, P. Deb, M.C. Chaturvedi, Coarsening behaviour of γ″-and γ'-particles in Inconel alloy 718, Metal Sci. 16 (1982) 555–561.
[30] C. Slama, C. Servant, G. Cizeron, Aging of the inconel 718 alloy between 500 and 750°C, J. Mater. Res. 12 (1997) 2298–2316.
[31] A. Devaux, L. Nazé, R. Molins, A. Pineau, A. Organista, J.Y. Guédou, J.F. Uginet, P. Héritier, Gamma double prime precipitation kinetic in alloy 718, Mater. Sci. Eng. A 486 (2008) 117–122.
[32] Y.Z. Ji, Y.C. Lou, M. Qu, J.D. Rowatt, F. Zhang, T.W. Simpson, L.Q. Chen, Predicting coherency loss of γ ″ precipitates in IN718 superalloy, Metall. Mater. Trans. A 47 (2016) 3235–3247.
[33] J.F. Nie, B.C. Muddle, Microstructural design of high-strength aluminum alloys, J. Phase Equilib. 19 (1998) 543–551.
[34] L. Kovarik, R.R. Unocic, J. Li, P. Sarosi, C. Shen, Y. Wang, M.J. Mills, Microtwinning and other shearing mechanisms at intermediate temperatures in Ni-based superalloys, Prog. Mater. Sci. 54 (2009) 839–873.
[35] W.J. Lu, X. Luo, Y.Q. Yang, K. Yan, B. Huang, P.T. Li, Nano-precipitates strengthened non-equiatomic medium-entropy alloy with outstanding tensile properties, Mater. Sci. Eng. A 780 (2020) 139218.
[36] J.F. Nie, Effects of precipitate shape and orientation on dispersion strengthening in magnesium alloys, Scr. Mater. 48 (2003) 1009–1015.
[37] R. Shi, N. Ma, Y. Wang, Predicting equilibrium shape of precipitates as function of coherency state, Acta Mater. 60 (2012) 4172–4184.